

Momentum anisotropy effects for quarkonium in a weakly-coupled quark-gluon plasma below the melting temperature

S. Biondini,¹ N. Brambilla,^{2,3} M. A. Escobedo,^{4,5} and A. Vairo²

¹*Albert Einstein Center, Institute for Theoretical Physics,
University of Bern, Sidlerstrasse 5, CH-3012 Bern, Switzerland*

²*Physik-Department, Technische Universität München,
James-Franck-Str. 1, 85748 Garching, Germany*

³*Institute for Advanced Study, Technische Universität München,
Lichtenbergstrasse 2 a, 85748 Garching, Germany*

⁴*Department of Physics, P.O. Box 35, 40014 University of Jyväskylä, Finland*

⁵*Institut de Physique Théorique, Université Paris Saclay, CNRS, CEA, F-91191 Gif-sur-Yvette, France*

(Dated: March 23, 2022)

In the early stages of heavy-ion collisions, the hot QCD matter expands more longitudinally than transversely. This imbalance causes the system to become rapidly colder in the longitudinal direction and a local momentum anisotropy appears. In this paper, we study the heavy-quarkonium spectrum in the presence of a small plasma anisotropy. We work in the framework of pNRQCD at finite temperature. We inspect arrangements of non-relativistic and thermal scales complementary to those considered in the literature. In particular, we consider temperatures larger and Debye masses smaller than the binding energy, which is a temperature range relevant for presently running LHC experiments. In this setting we compute the leading thermal corrections to the binding energy and the thermal width induced by quarkonium gluo-dissociation.

I. INTRODUCTION

In present day experiments at the Large Hadron Collider (LHC) and at the Relativistic Heavy Ion Collider (RHIC) a rich and broad program is ongoing to investigate QCD at finite temperature. The establishment of a hot QCD medium, dubbed as quark-gluon plasma (QGP), has been inferred thanks to the observation of at least two striking signatures: jet quenching and quarkonia suppression. In particular the latter, which has been proposed since long as a probe of the QGP formation [1], will be the subject of the present investigation.

Together with the experimental activity also the theoretical understanding of heavy quarkonia in medium has progressed significantly in the last years. A key to it has been the study of the heavy quark-antiquark potential in a thermal environment. The heavy quark-antiquark potential has been derived at high temperatures ($T \gg 1/r \gtrsim m_D$, where r is the quark-antiquark distance and m_D the Debye mass) in [2–4], and further computed in a wider range of temperatures in an effective field theory framework of QCD in the static limit [5] and for a large but finite heavy-quark mass [6]. The real part of the potential shows at high temperatures Debye screening, which is a source of quarkonium dissociation. The potential has also an imaginary part that stems from two further dissociation mechanisms: Landau damping [7, 8] and gluo-dissociation [9, 10].

A complete understanding of quarkonium in medium has to account for realistic QGP features. Among these is the momentum anisotropy of the thermal medium constituents. Indeed highly Lorentz contracted nuclei collide along the beam-axis, so that the longitudinal expansion of the hot QCD medium is more important than the radial expansion perpendicular to the beam axis (see,

e.g., [11]). At weak coupling this longitudinal expansion causes the system to quickly become much colder in the longitudinal than in the transverse direction, moreover the anisotropy can persist for a long time [12–16]. Recently the properties of an anisotropic QGP have been the subject of several investigations carried out in the framework of viscous hydrodynamics [17–21].

So far the effect of a local anisotropy on a quark-antiquark bound state has been taken into account via hard thermal loop (HTL) resummation of the gluon self energy, where a finite momentum anisotropy is assigned to the degrees of freedom entering the loops [22–24]. Numerical solutions of the Schrödinger equation for the bound state show that the anisotropy tends to decrease the effect of Landau damping and thus to increase the quarkonium melting temperature [25, 26], whereas analytical estimates are found in [24].

In this work, we assume the quarkonium to be a Coulombic system, so that its inverse size scales like $m\alpha_s$, and its typical binding energy like $m\alpha_s^2$, where m and α_s are the heavy-quark mass and strong coupling respectively. This is realized when $m\alpha_s$ is much larger than the temperature scale (moreover we consider negligible the effects of the hadronic scale Λ_{QCD}). In particular, we aim at investigating the heavy-quarkonium spectrum when the relevant scales, the non-relativistic and thermal ones, satisfy the following hierarchy

$$m \gg m\alpha_s \gg \pi T \gg m\alpha_s^2 \gg m_D, \Lambda_{\text{QCD}}, \quad (1)$$

and in the presence of a finite momentum anisotropy of the QGP constituents. In a weakly-coupled QGP, the Debye mass, m_D , scales like $m_D \sim gT$ and provides the inverse of an electric screening length. The hierarchy of scales (1) may be relevant for the $\Upsilon(1S)$, whose mass, inverse radius and binding energy are respectively

$m \approx 5$ GeV, $m\alpha_s \approx 1.5$ GeV and $m\alpha_s^2 \approx 0.5$ GeV [27]. In an expanding and then cooling QGP, the regime (1) is met at some point, say for $T \lesssim 2T_c \approx 0.3$ GeV for bottomonium. Note that this temperature is below the bottomonium melting temperature [28]. In so doing we partly generalize the study carried out in [6] for the isotropic case.

Since the quarkonium is assumed to be a Coulombic system, we do not include in the real part of the potential any term to model a (screened) long-range interaction (as done, e.g., in [26]). Such an inclusion would not be supported by the hierarchy of energy scales (1). The spectrum has also an imaginary part that provides the quarkonium width. In the situation of interest for this work, $m\alpha_s^2 \gg m_D$, gluo-dissociation is the dominant mechanism producing the thermal width. Such a mechanism has been reinterpreted as and connected to the singlet-to-octet break up in potential non-relativistic QCD (pNRQCD) at finite temperature in [29].

Following a common choice in the literature we implement a momentum anisotropy via distribution functions (B for Bose–Einstein, F for Fermi–Dirac) that read [17, 18]

$$f^{\text{B,F}}(\mathbf{q}, \xi) \equiv N(\xi) f_{\text{iso}}^{\text{B,F}}\left(\sqrt{\mathbf{q}^2 + \xi(\mathbf{q} \cdot \mathbf{n})^2}\right), \quad (2)$$

where ξ is the anisotropy parameter, $N(\xi) = \sqrt{1 + \xi}$ is a normalization factor that guarantees the same number of particles for the anisotropic and isotropic distribution functions and $f_{\text{iso}}^{\text{B,F}}(q)$ is understood to be either a Bose–Einstein or a Fermi–Dirac isotropic distribution for gluons and quarks respectively. Hence $f^{\text{B,F}}(\mathbf{q}, \xi)$ is obtained from the corresponding isotropic distribution by removing particles with a large momentum component along the anisotropy direction \mathbf{n} , and accordingly $\xi > 0$ parameterizes the anisotropy strength. The normalization factor $N(\xi)$ is often put to one in the literature, though its origin and impact have been discussed in [30]. As far as the present work is concerned, we keep the normalization factor in the following calculations.

The outline of the paper is the following: in Sec. II we compute the thermal modification of pNRQCD, pNRQCD_{HTL}, by integrating out the scale πT in the presence of a momentum anisotropy. At this stage and at our accuracy thermal effects are encoded in the singlet potential. In Sec. III we compute in pNRQCD_{HTL} the temperature-dependent real and imaginary parts of the quarkonium spectrum. The latter corresponds to the quarkonium thermal width. Conclusion and discussion are found in Sec. IV.

II. MATCHING pNRQCD TO pNRQCD_{HTL}

According to (1), one has to integrate out the heavy-quark mass and the typical momentum transfer before dealing with any thermal effect. Hence our starting point is pNRQCD, whose coefficients can be obtained at

zero temperature. The corresponding Lagrangian density reads as follows (we show only terms relevant for the present work) [31–33]:

$$\begin{aligned} \mathcal{L}_{\text{pNRQCD}} = & -\frac{1}{4}F_{\mu\nu}^a F^{a\mu\nu} + \sum_{i=1}^{n_f} \bar{q}_i i \not{D} q_i \\ & + \int d^3\mathbf{r} \text{Tr} \{S^\dagger (i\partial_0 - h_s) S + O^\dagger (iD_0 - h_o) O\} \\ & + \text{Tr} \{O^\dagger \mathbf{r} \cdot g\mathbf{E} S + S^\dagger \mathbf{r} \cdot \mathbf{E} O\} + \dots, \end{aligned} \quad (3)$$

where \mathbf{r} is the heavy quark-antiquark distance vector, $S = S\mathbb{1}_c/\sqrt{N_c}$ and $O = O^a T^a/\sqrt{T_F}$ are the heavy quark-antiquark color-singlet and color-octet fields respectively, q_i are n_f light quark fields taken massless, N_c is the number of colors, $T_F = 1/2$, and traces are understood over color and spin indices. We have taken the matching coefficients at leading order. The dots stand for higher-order terms in the multiple expansion and for octet-octet transitions that we do not need in the following. The singlet and octet Hamiltonians read

$$h_{s,o} = \frac{\mathbf{p}^2}{m} + V_{s,o}^{(0)} + \dots, \quad (4)$$

where $\mathbf{p} = -i\nabla_{\mathbf{r}}$ and the dots stand for higher-order terms in the $1/m$ expansion. The singlet and octet static potentials are at leading order in α_s : $V_s^{(0)} = -C_F\alpha_s/r$ and $V_o^{(0)} = \alpha_s/(2N_c r)$ respectively; $C_F = (N_c^2 - 1)/(2N_c)$ is the Casimir of the fundamental representation of $\text{SU}(N_c)$.

The computations that we are going to perform in this and in the next section share similarities with the ones done for quarkonium in a hot wind in the same temperature regime [34, 35]. In both cases we are dealing with a problem in which the distribution of particles in the medium has a preferred direction.

Thermal contributions to the real and imaginary parts of the heavy-quarkonium spectrum come from considering self-energy diagrams in pNRQCD and integrating them over momentum regions scaling respectively like the temperature and the binding energy. Integrating over the momentum region scaling like the temperature amounts at matching pNRQCD to another effective field theory, dubbed pNRQCD_{HTL} in [5, 6], where only modes with energy and momentum smaller than πT are dynamical. Thermal contributions are then encoded in the color-singlet potential of pNRQCD_{HTL}. We will consider integrating over the momentum region scaling like the binding energy in the next section.

The leading thermal contribution to the color-singlet potential comes from the self-energy diagram in Fig. 1, where the loop momentum is set to be $q \sim \pi T$. By using the vertices and propagators of the pNRQCD Lagrangian we obtain

$$\begin{aligned} \langle \Omega | T S(t, \mathbf{r}, \mathbf{R}) S^\dagger(0, \mathbf{0}, \mathbf{0}) | \Omega \rangle = & -4\pi\alpha_s C_F \\ & \times \int_{\mathbf{P}} e^{-iP_0 t + i\mathbf{P} \cdot \mathbf{R}} \langle \mathbf{r} | \frac{i}{P_0 - h_s + i\epsilon} r_i I_{ij} r_j \frac{i}{P_0 - h_s + i\epsilon} | \mathbf{0} \rangle, \end{aligned} \quad (5)$$

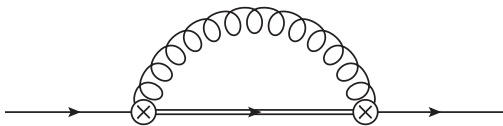


FIG. 1. Color-singlet self-energy diagram in pNRQCD. Single lines stand for quark-antiquark color-singlet propagators, double lines for color-octet propagators, curly lines for gluons and a circle with a cross for a chromoelectric dipole vertex.

where T stands for time ordering, $\int_P \equiv \int d^4P/(2\pi)^4$, $P^\mu = (P^0, \mathbf{P})$ and $|\Omega\rangle$ is the ground state of the theory. The thermal part of the self-energy loop integral, I_{ij} , is given by

$$I_{ij} = \int_q \frac{i(q_0)^2 2\pi \delta(q^2)}{P_0 - q_0 - h_o + i\epsilon} \left(\delta_{ij} - \frac{q_i q_j}{|\mathbf{q}|^2} \right) f^B(\mathbf{q}, \xi). \quad (6)$$

We have to separate terms that go into the wave-function renormalization from those that go into the color-singlet potential of pNRQCD_{HTL}. To this end we rewrite $P^0 - h_o = P^0 - h_s - \Delta V$, where $\Delta V = (h_o - h_s) = (N_c \alpha_s)/(2r) + \dots$, and, due to the condition $q \sim \pi T$ that sets the loop momentum to be much larger than the energy of the heavy quark-antiquark pair, we expand the octet propagator in (6). After dropping terms that go into the wave-function renormalization, the part of $r_i I_{ij} r_j$ that contributes to the color-singlet potential of pNRQCD_{HTL} reads

$$r_i I_{ij} r_j \Big|_{q \sim \pi T}^{\text{contr. to } V_s} = i \left(\frac{2}{m} + \Delta V r^2 \right) \int_q 2\pi \delta(q^2) f^B(\mathbf{q}, \xi) - i(\Delta V r_i r_j) \int_q 2\pi \delta(q^2) \frac{q_i q_j}{|\mathbf{q}|^2} f^B(\mathbf{q}, \xi). \quad (7)$$

To match onto pNRQCD_{HTL} we compute the correlator $\langle \Omega | T S(t, \mathbf{r}, \mathbf{R}) S^\dagger(0, \mathbf{0}, \mathbf{0}) | \Omega \rangle$ in pNRQCD_{HTL} and require this expression to be equal to (5). The color-singlet potential of pNRQCD_{HTL} turns out to be the same as in pNRQCD plus a thermal correction δV_s that reads

$$\delta V_s = -i4\pi\alpha_s C_F r_i I_{ij} r_j \Big|_{q \sim \pi T}^{\text{contr. to } V_s}. \quad (8)$$

The integral can be easily evaluated and the final result for the anisotropic potential at finite temperature is

$$\delta V_s = \frac{2\pi\alpha_s C_F T^2}{3m} \mathcal{F}_1(\xi) + \frac{\pi\alpha_s^2 C_F N_c T^2 r}{12} \mathcal{F}_2(\xi) + \frac{\pi\alpha_s^2 C_F N_c T^2 (\mathbf{r} \cdot \mathbf{n})^2}{12r} \mathcal{F}_3(\xi), \quad (9)$$

where the definitions of the functions embedding the anisotropy parameter are

$$\mathcal{F}_1(\xi) = N(\xi) \frac{\arctan \sqrt{\xi}}{\sqrt{\xi}}, \quad (10)$$

$$\mathcal{F}_2(\xi) = N(\xi) \left(\frac{\arctan \sqrt{\xi}}{\sqrt{\xi}} + \frac{1}{\xi} - \frac{\arctan \sqrt{\xi}}{\xi \sqrt{\xi}} \right), \quad (11)$$

$$\mathcal{F}_3(\xi) = N(\xi) \left(\frac{\arctan \sqrt{\xi}}{\sqrt{\xi}} - \frac{3}{\xi} + \frac{3 \arctan \sqrt{\xi}}{\xi \sqrt{\xi}} \right). \quad (12)$$

We comment briefly about the result: first, at this order no imaginary part, and hence no thermal width, arises; second, for $\xi \rightarrow 0$ the result in (9) agrees with the isotropic case derived in [6]. Finally, we notice that the term in the second line in (9) is of order ξ when expanding for a small anisotropy parameter, signaling that its origin is entirely due to the breaking of the spherical symmetry of the parton momentum distribution.

III. THERMAL CORRECTIONS TO THE SPECTRUM

In our setting the next relevant scale after the temperature is the quarkonium binding energy. The process we are looking at is again a singlet-to-octet transition, however with energy and momenta scaling like $m\alpha_s^2$ rather than πT . This contribution is not part of the potential but comes as a low-energy correction to the spectrum of pNRQCD_{HTL}. It may be computed at leading order from the one-loop diagram in Fig. 1, where now, however, the typical loop momentum is selected to be of order $m\alpha_s^2$. To ensure that we are computing only contributions from the momentum region $q \sim m\alpha_s^2 \ll \pi T$, we need to expand the anisotropic distribution function

$$f^B(\mathbf{q}, \xi) = \left(e^{\frac{|\mathbf{q}|}{T} \sqrt{1+\xi\lambda^2}} - 1 \right)^{-1} \approx \frac{T}{|\mathbf{q}| \sqrt{1+\xi\lambda^2}}, \quad (13)$$

where $\lambda = \mathbf{q} \cdot \mathbf{n}/|\mathbf{q}|$ is the cosine of the angle between the gluon momentum and the anisotropy direction. We keep only the leading term in the $|\mathbf{q}|/T$ expansion. Differently from the calculation in Sec. II, we cannot expand the octet propagator. Then the contribution from the momentum region $q \sim m\alpha_s^2$ to the self-energy diagram in Fig. 1 reads

$$\delta \Sigma = -i4\pi\alpha_s C_F r_i I_{ij} r_j \Big|_{q \sim m\alpha_s^2}, \quad (14)$$

where

$$r_i I_{ij} r_j \Big|_{q \sim m\alpha_s^2} = T r_i \int_q \frac{i(q_0)^2 2\pi \delta(q^2)}{P_0 - q_0 - h_o + i\epsilon} \left(\delta_{ij} - \frac{q_i q_j}{|\mathbf{q}|^2} \right) \times \frac{r_j}{|\mathbf{q}| \sqrt{1+\xi\lambda^2}}. \quad (15)$$

The integral (15) has a vanishing imaginary part. This means that there is no contribution coming from $\delta \Sigma$, as defined in (14), to the real part of the spectrum. Hence, the thermal shift in the binding energy is entirely due to the shift in the singlet potential, δV_s , computed previously in (9). We can write it as

$$\delta E_{\text{bind}} = \langle n l m | \delta V_s | n l m \rangle, \quad (16)$$

where $|n l m\rangle$ are eigenstates of the singlet Hamiltonian h_s , with quantum numbers n , l (orbital angular momentum) and m (orbital angular momentum along the z direction). Since, according to our hierarchy of energy

scales, the potential entering h_s is the Coulomb potential, the states $|nlm\rangle$ are just Coulombic bound states. At leading accuracy, δE_{bind} then reads

$$\begin{aligned} \delta E_{\text{bind}} = & \frac{2\pi\alpha_s C_F T^2}{3m} \mathcal{F}_1(\xi) \\ & + \frac{\pi\alpha_s N_c T^2}{12m} [3n^2 - l(l+1)] \left(\mathcal{F}_2(\xi) + \frac{\mathcal{F}_3(\xi)}{3} \right. \\ & \left. + \frac{2}{3} \mathcal{F}_3(\xi) C_{2100}^{l0} C_{210m}^{lm} \right), \end{aligned} \quad (17)$$

where the Clebsch–Gordan coefficients are understood with the notation $C_{j_1 j_2 m_1 m_2}^{JM}$ ($C_{j_1 j_2 m_1 m_2}^{JM} = 0$ if $J > j_1 + j_2$ or $J < |j_1 - j_2|$).

ξ	$\mathcal{F}_1(\xi)$	$\mathcal{F}_2(\xi)$	$\mathcal{F}_3(\xi)$	$\mathcal{G}_1(\xi)$	$\mathcal{G}_2(\xi)$
0.1	1.016	1.346	0.026	1.032	0.009
0.3	1.043	1.367	0.072	1.089	0.026
0.5	1.067	1.383	0.114	1.141	0.041
1	1.110	1.414	0.200	1.246	0.077

TABLE I. The anisotropy functions defined in (10)-(12), (20) and (21) for some values of ξ .

The integral (15) has a non-vanishing real part that contributes to the imaginary part of $\delta\Sigma$. The imaginary part of the self energy gives rise to a thermal width:

$$\begin{aligned} \Gamma = & -2\langle nlm | \text{Im}(\delta\Sigma) | nlm \rangle \\ = & 8\pi^2 \alpha_s C_F T \langle nlm | r_i \int_q \frac{\delta(E_n + q_0 - h_o) q_0^2}{|\mathbf{q}| \sqrt{1 + \xi \lambda^2}} \\ & \times \left(\delta_{ij} - \frac{q_i q_j}{|\mathbf{q}|^2} \right) (2\pi) \delta(q^2) r_j | nlm \rangle, \end{aligned} \quad (18)$$

where $E_n = -m(C_F \alpha_s)^2 / (4n^2)$ is the energy of the bound state. The final result reads

$$\begin{aligned} \Gamma = & \frac{4}{3} \alpha_s^3 T \left(\frac{C_F N_c^2}{4} + \frac{C_F^2 N_c}{n^2} + \frac{C_F^3}{n^2} \right) \mathcal{G}_1(\xi) \\ & + \alpha_s^3 T \left(\frac{C_F N_c^2}{4} - \frac{C_F^2 N_c}{2n^2} + \frac{C_F^3}{n^2} \right) \mathcal{G}_2(\xi) C_{2100}^{l0} C_{210m}^{lm}, \end{aligned} \quad (19)$$

where the anisotropy functions are in this case

$$\mathcal{G}_1(\xi) = N(\xi) \frac{\text{arcsinh}(\sqrt{\xi})}{\sqrt{\xi}}, \quad (20)$$

$$\mathcal{G}_2(\xi) = N(\xi) \frac{(1 + 2\xi/3) \text{arcsinh}(\sqrt{\xi}) - \sqrt{\xi(1 + \xi)}}{\sqrt{\xi^3}}. \quad (21)$$

The appearance of a thermal width follows from the fact that the singlet-to-octet transition becomes a real process if the emitted gluon has an energy of the order of the binding energy.

The limit $\xi \rightarrow 0$ corresponds to the isotropic case. For $\xi \rightarrow 0$, we have that $\mathcal{F}_1(\xi) \rightarrow 1$, $\mathcal{F}_2(\xi) \rightarrow 4/3$, $\mathcal{G}_1(\xi) \rightarrow 1$,

whereas both $\mathcal{F}_3(\xi)$ and $\mathcal{G}_2(\xi)$ vanish linearly in ξ . In this limit both the binding energy (17) and the thermal width (19) reduce to previously known expressions found in [6]. In Tab. I we show some benchmark values of the anisotropy functions.

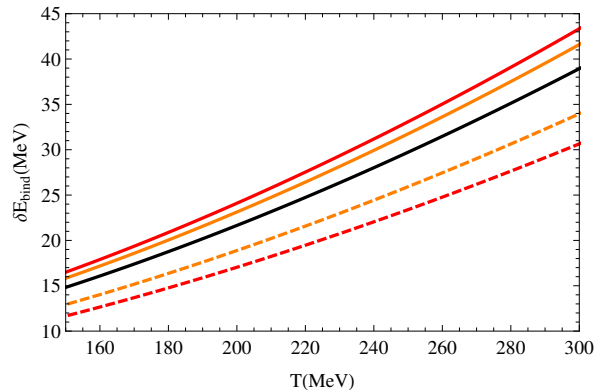


FIG. 2. (Color Online) Binding-energy shift of a $1S$ ($n = 1, l = 0$) bottomonium state according to (17). We show the binding-energy shift for the isotropic case, black solid line, and for two different values of the anisotropy parameter $\xi = 0.5$ and $\xi = 1$ in orange and red solid (dashed) lines respectively when the normalization factor is $N(\xi) = \sqrt{1 + \xi}$ ($N(\xi) = 1$). For all the figures (here and in the following) we have taken $\alpha_s(2\pi T)$ and considered it running at one loop with three quark flavours. The bottom-quark mass has been chosen to be half of the $\Upsilon(1S)$ mass, i.e., 4730 MeV.

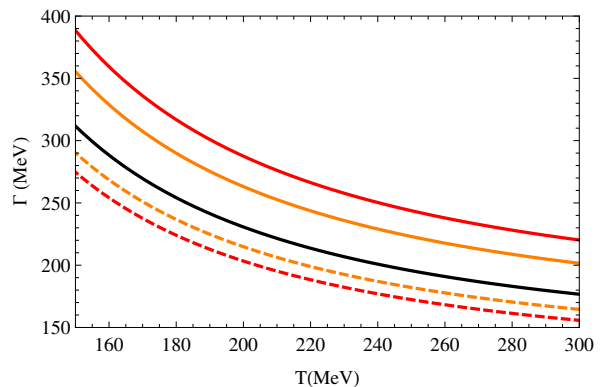


FIG. 3. (Color Online) Thermal width of a $1S$ ($n = 1, l = 0$) bottomonium state according to (19). The different curves are defined as in Fig. 2.

IV. CONCLUSION AND DISCUSSION

In an early stage, heavy-ion collisions are characterized by parton momentum anisotropies. Accordingly the evolution of the fireball is described in terms of viscous and anisotropic hydrodynamical models. Due to the fact that hard probes, like heavy quarkonia, get formed in such an early stage of the heavy ion-collisions and experience the

medium until late times, their dynamics has to account for an anisotropic momentum distribution of the QGP constituents. In this paper, we have derived for the hierarchy of scales (1) and at leading order the real and imaginary thermal parts of the quarkonium spectrum in an anisotropic QGP. The imaginary part originates from the quarkonium gluo-dissociation in the medium. Our result complements previous studies for an anisotropic plasma where the real and imaginary part of the quark-antiquark potential were obtained for a temperature scale larger than the inverse radius of the bound state. In so doing we extend the knowledge of a weakly-coupled quarkonium to temperature ranges that may be reached during the QGP evolution at present day colliders.

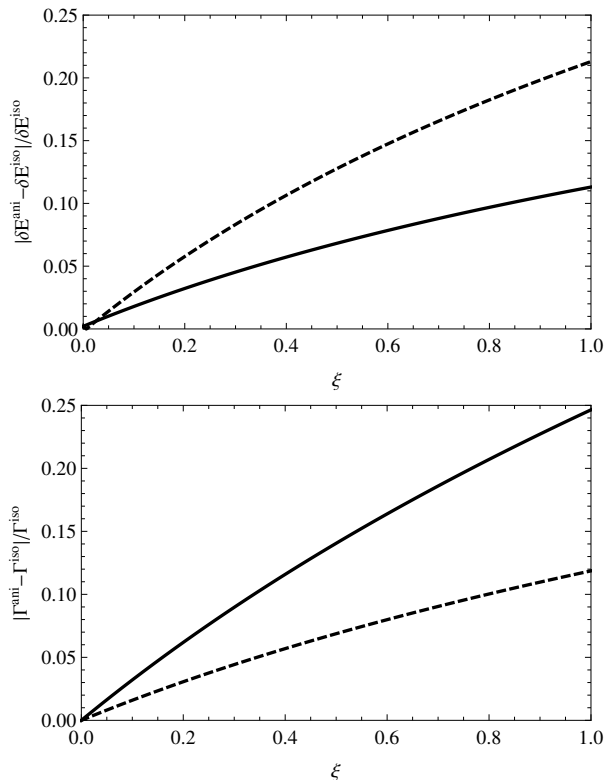


FIG. 4. Relative change in the binding energy (upper plot) and thermal width (lower plot) due to the presence of a momentum anisotropy. δE^{ani} is the binding-energy shift in (17) evaluated for $\xi \neq 0$, whereas δE^{iso} is the binding-energy shift in (17) evaluated at $\xi = 0$, for a $1S$ bottomonium state. In a similar way we have defined the thermal widths, Γ^{ani} and Γ^{iso} , taken from (19). For solid (dashed) lines the normalization has been taken $N(\xi) = \sqrt{1+\xi}$ ($N(\xi) = 1$).

The real thermal part of the spectrum comes from thermal corrections to the potential defined in the context of pNRQCD_{HTL}. They are encoded in the self-energy diagram of Fig. 1 evaluated at the temperature scale. The result is given in (9). Thermal corrections to the potential are proportional to the square of the temperature and, as discussed elsewhere, do not show Debye screening [5, 6]. The corresponding expectation

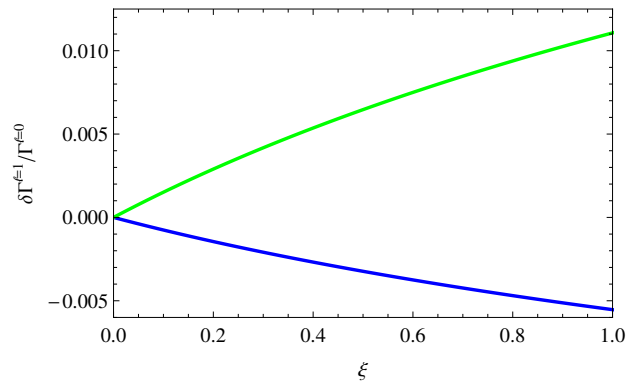


FIG. 5. (Color Online) Ratio of the differences between the thermal corrections to the widths of $1P$ ($n = 2, l = 1$) and $2S$ ($n = 2, l = 0$) bottomonium states and the $2S$ -state thermal width, respectively second and first line in (19), as a function of ξ . The blue (lower) line refers to the $m = \pm 1$ states whereas the green (upper) line to the $m = 0$ one.

value provides the real part of the thermal corrections to the binding energy. They are given in (17). In Fig. 2 we show the binding-energy shift for a $1S$ bottomonium state in the isotropic case, $\xi = 0$, and in the case of a finite momentum anisotropy, $\xi = 0.5$ and $\xi = 1$. We see that the impact of an anisotropic plasma crucially depends on the normalization factor, either $N(\xi) = 1$ or $N(\xi) = \sqrt{1+\xi}$, respectively shown in dashed and solid lines. For $N(\xi) = 1$ the anisotropy reduces the thermal correction to the binding energy, whereas for $N(\xi) = \sqrt{1+\xi}$ it increases it.

The computation of the spectrum in pNRQCD_{HTL} leads also to an imaginary part coming from the self-energy diagram of Fig. 1 evaluated at the binding-energy scale. The imaginary part may be understood as a thermal width, whose explicit expression is in (19). In Fig. 3 we show the thermal width for a $1S$ bottomonium state in the isotropic case, $\xi = 0$, and in the case of a finite momentum anisotropy, $\xi = 0.5$ and $\xi = 1$. Also here the size and sign of the thermal corrections strongly depend on the normalization factor, either $N(\xi) = 1$ or $N(\xi) = \sqrt{1+\xi}$, respectively shown in dashed and solid lines. Although the dependence on the anisotropy is qualitatively similar in the binding energy and thermal width, we find that the effect of the anisotropy is more important for the binding energy with respect to the thermal width when $N(\xi) = 1$ (see dashed lines in Fig. 4), whereas the opposite is true when $N(\xi) = \sqrt{1+\xi}$ (see solid lines in Fig. 4).

Finally, we comment on the effect of an anisotropic QGP on the bound-state polarization. In Fig. 5 we show the differences between the thermal corrections to the widths of $1P$ and $2S$ bottomonium states. For $\xi \leq 1$ such differences are typically of the order of few per mill (at most 1%) with respect to the corresponding $2S$ state thermal width. This suppression is due to various effects: the ratio between the anisotropy functions \mathcal{G}_2 and \mathcal{G}_1 , see

the benchmark values in Tab. I, the combination involving the color factors N_c and C_F , and the Clebsch–Gordan coefficients. We conclude that for small anisotropies the effect of an anisotropic QGP on the bound-state polarization is tiny and possibly phenomenologically irrelevant.

ACKNOWLEDGEMENTS

The work of S.B. was partly supported by the Swiss National Science Foundation (SNF) under grant 200020-168988. N.B. and A.V. acknowledge support from the DFG grant BR 4058/1-2 “Effective field theories for hard probes of hot plasma” and the DFG cluster of excellence “Origin and structure of the universe” (www.universe-cluster.de). The work of M.A.E. was supported by the European Research Council under the Advanced Investigator Grant ERC-AD-267258 and by the Academy of Finland, project 303756.

-
- [1] T. Matsui and H. Satz, *Phys. Lett.* **B178**, 416 (1986).
- [2] M. Laine, O. Philipsen, P. Romatschke, and M. Tassler, *JHEP* **03**, 054 (2007), arXiv:hep-ph/0611300 [hep-ph].
- [3] M. Laine, *JHEP* **05**, 028 (2007), arXiv:0704.1720 [hep-ph].
- [4] Y. Burnier, M. Laine, and M. Vepsalainen, *JHEP* **01**, 043 (2008), arXiv:0711.1743 [hep-ph].
- [5] N. Brambilla, J. Ghiglieri, A. Vairo, and P. Petreczky, *Phys. Rev.* **D78**, 014017 (2008), arXiv:0804.0993 [hep-ph].
- [6] N. Brambilla, M. A. Escobedo, J. Ghiglieri, J. Soto, and A. Vairo, *JHEP* **09**, 038 (2010), arXiv:1007.4156 [hep-ph].
- [7] L. Grandchamp and R. Rapp, *Phys. Lett.* **B523**, 60 (2001), arXiv:hep-ph/0103124 [hep-ph].
- [8] L. Grandchamp and R. Rapp, *Nucl. Phys.* **A709**, 415 (2002), arXiv:hep-ph/0205305 [hep-ph].
- [9] D. Kharzeev and H. Satz, *Phys. Lett.* **B334**, 155 (1994), arXiv:hep-ph/9405414 [hep-ph].
- [10] X.-M. Xu, D. Kharzeev, H. Satz, and X.-N. Wang, *Phys. Rev.* **C53**, 3051 (1996), arXiv:hep-ph/9511331 [hep-ph].
- [11] M. Strickland, *Acta Phys. Polon.* **B45**, 2355 (2014), arXiv:1410.5786 [nucl-th].
- [12] W. Israel, *Annals Phys.* **100**, 310 (1976).
- [13] G. Baym, *Phys. Lett.* **B138**, 18 (1984).
- [14] M. Martinez and M. Strickland, *Phys. Rev.* **C79**, 044903 (2009), arXiv:0902.3834 [hep-ph].
- [15] W. Florkowski and R. Ryblewski, *Phys. Rev.* **C83**, 034907 (2011), arXiv:1007.0130 [nucl-th].
- [16] M. Martinez and M. Strickland, *Nucl. Phys.* **A848**, 183 (2010), arXiv:1007.0889 [nucl-th].
- [17] P. Romatschke and M. Strickland, *Phys. Rev.* **D68**, 036004 (2003), arXiv:hep-ph/0304092 [hep-ph].
- [18] P. Romatschke and M. Strickland, *Phys. Rev.* **D70**, 116006 (2004), arXiv:hep-ph/0406188 [hep-ph].
- [19] S. Mrowczynski, A. Rebhan, and M. Strickland, *Phys. Rev.* **D70**, 025004 (2004), arXiv:hep-ph/0403256 [hep-ph].
- [20] M. Nopoush, M. Strickland, and R. Ryblewski, (2016), arXiv:1610.10055 [nucl-th].
- [21] M. Nopoush, R. Ryblewski, and M. Strickland, *Phys. Rev.* **C90**, 014908 (2014), arXiv:1405.1355 [hep-ph].
- [22] A. Dumitru, Y. Guo, and M. Strickland, *Phys. Lett.* **B662**, 37 (2008), arXiv:0711.4722 [hep-ph].
- [23] A. Dumitru, Y. Guo, and M. Strickland, *Phys. Rev.* **D79**, 114003 (2009), arXiv:0903.4703 [hep-ph].
- [24] Y. Burnier, M. Laine, and M. Vepsalainen, *Phys. Lett.* **B678**, 86 (2009), arXiv:0903.3467 [hep-ph].
- [25] A. Dumitru, Y. Guo, A. Mocsy, and M. Strickland, *Phys. Rev.* **D79**, 054019 (2009), arXiv:0901.1998 [hep-ph].
- [26] M. Margotta, K. McCarty, C. McGahan, M. Strickland, and D. Yager-Elorriaga, *Phys. Rev.* **D83**, 105019 (2011), [Erratum: *Phys. Rev.* **D84**, 069902(2011)], arXiv:1101.4651 [hep-ph].
- [27] A. Vairo, *AIP Conf. Proc.* **1317**, 241 (2011), arXiv:1009.6137 [hep-ph].
- [28] M. A. Escobedo and J. Soto, *Phys. Rev.* **A78**, 032520 (2008), arXiv:0804.0691 [hep-ph].
- [29] N. Brambilla, M. A. Escobedo, J. Ghiglieri, and A. Vairo, *JHEP* **12**, 116 (2011), arXiv:1109.5826 [hep-ph].
- [30] O. Philipsen and M. Tassler, (2009), arXiv:0908.1746 [hep-ph].
- [31] A. Pineda and J. Soto, *Nucl. Phys. Proc. Suppl.* **64**, 428 (1998), arXiv:hep-ph/9707481 [hep-ph].
- [32] N. Brambilla, A. Pineda, J. Soto, and A. Vairo, *Nucl. Phys.* **B566**, 275 (2000), arXiv:hep-ph/9907240 [hep-ph].
- [33] N. Brambilla, A. Pineda, J. Soto, and A. Vairo, *Rev. Mod. Phys.* **77**, 1423 (2005), arXiv:hep-ph/0410047 [hep-ph].
- [34] M. A. Escobedo, J. Soto, and M. Mannarelli, *Phys. Rev.* **D84**, 016008 (2011), arXiv:1105.1249 [hep-ph].
- [35] M. A. Escobedo, F. Giannuzzi, M. Mannarelli, and J. Soto, *Phys. Rev.* **D87**, 114005 (2013), arXiv:1304.4087 [hep-ph].